University of Nebraska - Lincoln

DigitalCommons@University of Nebraska - Lincoln

2019

Unmanned aerial system and satellite-based high resolution imagery for high-throughput phenotyping in dry bean

Sindhu Sankaran

Juan José Quirós

Phillip N. Miklas

Unmanned aerial system and satellite-based high resolution imagery for high-throughput phenotyping in dry bean

Sindhuja Sankaran[a,*,1], Juan José Quirós[a,1], Phillip N. Miklas[b]

[a] Department of Biological System Engineering, Washington State University, PO Box 646120, Pullman, WA, United States
[b] USDA–ARS, Grain Legume Genetics and Physiology Research Unit, 24106 N. Bunn Rd., Prosser, WA, United States

A B S T R A C T

Dry bean breeding programs are crucial to improve the productivity and resistance to biotic and abiotic stress. Phenotyping is a key process in breeding that refers to crop trait evaluation. In recent years, high-throughput plant phenotyping methods are being developed to increase the accuracy and efficiency for crop trait evaluations. In this study, aerial imagery at different resolutions were evaluated to phenotype crop performance and phenological traits using genotypes from two breeding panels, Durango Diversity Panel (DDP) and Andean Diversity Panel (ADP). The unmanned aerial system (UAS) based multispectral and thermal data were collected for two seasons at multiple time points (about 50, 60 and 75 days after planting/DAP in 2015; about 60 and 75 DAP in 2017). Four image-based features were extracted from multispectral images. Among different features, normalized difference vegetation index (NDVI) data were found to be consistently highly correlated with performance traits (above ground biomass, seed yield), especially during imaging at about 60–75 DAP (early pod development). Overall, correlations were higher using NDVI in ADP than DDP with biomass ($r = -0.67$ to -0.91 in ADP; $r = -0.55$ to -0.72 in DDP) and seed yield ($r = 0.51$ to 0.73 in ADP; $r = 0.42$ to 0.58 in DDP) at about 60 and 75 DAP. For thermal data, a temperature data normalization (utilizing common breeding plots in multiple thermal images) was implemented and the MEAN plot temperatures generally correlated significantly with biomass ($r = 0.28$–0.88). Finally, lower resolution satellite images (0.05–5 m/pixel) using UAS data was simulated and image resolution beyond 50 cm was found to reduce the relationship between image features (NDVI) and performance variables (biomass, seed yield). Four different high resolution satellite images: Pleiades-1A (0.5 m), SPOT 6 (1.5 m), Planet Scope (3.0 m), and Rapid Eye (5.0 m) were acquired to validate the findings from the UAS data. The results indicated sub-meter resolution satellite multispectral imagery showed promising application in field phenotyping, especially when the genotypic responses to stress is prominent. The correlation between NDVI extracted from Pleiades-1A images with seed yield ($r = 0.52$) and biomass ($r = -0.55$) were stronger in ADP; where the strength in relationship reduced with decreasing satellite image resolution. In future, we anticipate higher spatial and temporal resolution data achieved with low-orbiting satellites will increase applications for high-throughput crop phenotyping.

1. Introduction

United States is one of the top ten dry bean (*Phaseolus vulgaris* L.) producing countries in the world. Dry bean is important in human nutrition because it is high in nutrients (folate, manganese, potassium, vitamin B6), dietary fiber, and protein (Petry et al., 2015; Miklas et al., 2006). This nutritional impact is important for both developed and developing countries; but especially the latter, where dry bean provides basic nutrition for the populace. Dry bean breeding programs are consistently directed towards improving yield potential and developing

varieties tolerant to stressful conditions caused by diseases, edaphic factors, and drought (Miklas et al., 2006; Beebe et al., 2013). Among different stressors, drought (second to diseases) is known to reduce yields from 10% to 100% (Rao, 2014; Polania, et al., 2016).

In plant breeding, field phenotyping refers to systematic plot-level qualitative or quantitative evaluation of crop traits. Phenotyping is commonly performed manually and can be time-consuming with acquisition of low spatial and temporal information (Sankaran et al., 2015a). To maximize breeding efficiency, new plant phenotyping tools must be adopted to match the advancements in quality high-throughput

---

genotyping tools. Recently, field-based high-throughput plant phenotyping (HTPP) techniques have advanced through the use of proximal and remote sensing platforms (Andrade-Sanchez et al., 2014; Zaman-Allah et al., 2015; Holman et al., 2016).

Several efforts using remote sensing for HTPP of bean plants have been reported. In field conditions, strong correlations between sensor features and yield potential were detected during both flowering and pod filling stages (Rajah et al., 2017). Using a hyperspectral system, Gutierrez et al. (2006) studied the relation between green normalized difference vegetation index (GNDVI) and yield based on phosphorus application rates, and found that GNDVI decreased near physiological maturity. Other reports involving remote sensing methods for disease monitoring (Boechat et al., 2014), evaluation of drought and low nitrogen responses (Sankaran et al., 2018), and determination of nitrogen/chlorophyll levels (Abrahão et al., 2013) in bean plants have been reported.

The use of unmanned aerial system (UAS) to capture low altitude high resolution imagery allows the acquisition of homogeneous information at a given time point with quick capture of data from multiple plots. RGB cameras have been widely used for field plant phenotyping in multiple crops (e.g. Sugiura et al., 2016; Hu et al., 2018; Reza et al., 2018), aimed towards assessing multiple crop traits. Thermal data has also been explored to analyze water use efficiency and water stress in plants (Jones et al., 2009; Gomez-Candon et al., 2016; Ludovisi et al., 2017). The applications of UAS-based sensor data for HTPP is rising with the development of user-friendly platforms and sensors, alongside software packages with image processing capabilities.

In recent years, emergence of low orbiting satellites (LOS) with high spatial and temporal resolution (Onojeghuo et al., 2018) have broadened the application of remote sensing in agriculture. Some of the available high-resolution satellite imagery is summarized in Supplementary Materials, Table S1. The availability of sub-meter spatial resolution multispectral data from LOS, with a desired re-visit time, could enhance field-based HTPP capabilities, where the breeding plots are in the range of a few square meters in size. Moreover, LOS data can easily capture data from multiple locations as often breeding trials involves multiple sites to evaluate genotype-environment interactions.

LOS images are being used for multiple agricultural applications, such as to predict crop yield (Zhao et al., 2015), evaluate heterogeneity in field crops (Schwalbert et al., 2018), and to detect water logging in winter wheat production during booting stage (Liu et al., 2018). Sub-meter multispectral imagery from LOS offers a variety of remote sensing applications similar to UAS images. However, uncertainty on the reliability and utilization of such data in various agricultural applications remains. To the best of our knowledge, applications of LOS imagery for phenotyping applications in plant breeding trials are absent. Thus, with an overall goal to evaluate and establish remote sensing methods for high-throughput plant phenotyping in dry bean breeding nurseries, our specific objectives were to: (1) evaluate the sensitivity of genotypes to stress using UAS-based multispectral imaging with crop performance and other phenological traits in breeding trials as a reference; (2) introduce novel approaches to calibrate thermal images to compensate for inter-imagery dynamic temperature differences for phenotyping applications, and (3) evaluate the application of LOS data for dry bean HTPP.

2. Materials and methods

2.1. Study area, genotypes, and ground reference data

The field site was at the Washington State University's Roza Research Farm in Prosser, WA (46°29′N, 119°73′W), which has a Warden (coarse-silty, mixed, superactive, mesic, Xeric Haplocambid) soil type. During two seasons, 2015 and 2016 (Supplementary Materials, Fig. S1), multiple stress (low fertility with low N and P, intermittent drought, soil compaction, and high root rot incidence) was

imposed on genotypes representing the Durango Diversity Panel (DDP) and Andean Diversity Panel (ADP). The research site referred to as the 'purgatory plot' is used to develop dry bean germplasm with broad adaptation by identifying breeding lines with tolerance to multiple stresses. Multiple stress is induced by never fertilizing to generate low N and low P conditions; deficit irrigation at 30% evapotranspiration applied by overhead sprinklers once a week to simulate intermittent drought; reduced tillage to promote soil compaction; and a short crop rotation alternating wheat and dry bean to promote buildup of soil root rotting pathogens, namely *Fusarium solani* (Mart.) Sacc. species complex. An average rainfall of 50 mm during the growing season helps to realize drought stress. Pre-plant and post emergence herbicides, in addition to hand hoeing later in the season, were used to control weeds. In general, N and P fertility in 2015 season was higher than 2016 season (dry bean crop preceded wheat crop). The soil data is summarized in Supplementary Materials, Table S2. In regard to the growing season stress levels, crops grown in 2015 experienced less stress (more available nutrients, early planting dates, less heat incidents) than those grown in 2016. The goal was to evaluate crop responses to multiple stressors and individual effects were not assessed.

The DDP consists of dry bean genotypes (primarily cultivars but also landraces and germplasm releases) representing market classes (pinto, pink, small red, great northern) originating from Race Durango within the Middle American gene pool (Singh et al., 1991). The DDP genotypes are well adapted to the Pacific Northwest (PNW). The ADP genotypes representing kidney, yellow, red mottled, and cranberry market classes used in this study were selected based on adaptation to the PNW from a broader collection of 397 Andean genotypes from across the world (Cichy et al., 2015). The DDP and ADP were purposely comprised of stress tolerant and susceptible genotypes to promote evaluation of stress response.

An individual plot representing a single genotype was comprised of 4 rows of 3 m length and 0.55 m row spacing. Target seeding rate was 285,000 plants ha^{-1}. The experiments were planted in a randomized complete block design (RCBD). In 2015, 192 genotypes of DDP were evaluated with two replications (15–01 and 15–02). For ADP, three replications (15–03, 15–04 and 15–05) of 64 genotypes were assessed. In 2016, two replications of 74 genotypes of DDP (16–01 and 16–02) and 45 genotypes of ADP (16–03 and 16–04) were evaluated (Table 1). In 2016, seven other distinct smaller breeding nurseries with fewer genotypes were planted, but are not included in this study. The total number of plots analyzed in 2015 and 2016 was 576 and 480, respectively.

The ground reference data collected during this study that were compared to remote sensing data included: emergence, days to flowering (DF), days to harvest maturity (DHM), canopy height (CH), biomass rating, and seed yield. Emergence was scored from 1 (complete) to 9 (no plants) at early seedling stage (V1 to V2) and estimates stand establishment within a plot. DF represents the number of days after planting (DAP, also stated as days after sowing) to when 50% of the plants within a plot had at least one open blossom. DHM represented

Table 1
Year, number of genotypes, and diversity panel used in this study.

Experiment-replication	Year	Number of genotypes	Panel
15–01	2015	192	DDP
15–02		192	
15–03	2015	64	ADP
15–04		64	
15–05		64	
16–01	2016	74	DDP
16–02		74	
16–03	2016	45	ADP
16–04		45	

the number of days after planting to when 90% of the plants within a plot were ready to be harvested. CH was measured in cm at mid-pod fill stage (R4) as an average of CH across the plot. Above ground canopy biomass was visually rated from 1 (complete row closure and densest canopy with minimal porosity) to 9 (no plants) at pod fill (R4) to estimate the relative amount of above ground plant biomass (e.g. 3 for plants that were 40–45 cm tall, 75% closed rows, dense canopy; 5 for plants that were 30–40 cm tall, 50% closed rows, 50% light penetration; and 7 for plants that were 20–30 cm tall, 25% closed rows, 75% light penetration) in a given plot. Further details with pictures are available in Trapp (2015) and Trapp et al. (2016). The dry bean vegetative growth stages were defined based on Schwartz and Langham (2010) and Manitoba Pulse and Soybean Growers (2019). Harvested seed from the central two rows was used to estimate plot yield (kg ha^{-1}).

2.2. UAS data acquisition

A three-band modified multispectral camera of 16 megapixel (8-bit) was used (Canon Powershot ELPH 340 HS, LDC LLC, Carlstadt, New Jersey, United States) to capture multispectral images. The camera captures red (R, 550–710 nm), green (G, 500–620 nm), and near infrared (NIR, 800–900 nm) bands. For thermal data collection, a FLIR Tau 2 640 (Mtech Imaging USA LLC, Dallas, Texas, United States) was used; which captures emission in spectral range from 7.5 to 13.5 μm. The sensors were placed on the gimbal of an octocopter model OktoXL 6S12 (HiSystems GmbH, Moormerland, Germany). The UAS was powered by a 6500 mAh Lithium-ion polymer battery. All data collection dates were under sunny conditions (between 10 am and 2 pm).

Images were captured at 120 m above ground level. A reference white panel of 25 × 25 cm (Spectralon Reflectance Target, CSTM-SRT-99–100, Spectra Vista Cooperation, New York, USA) was imaged for subsequent radiometric correction. The firmware of the multispectral camera was configured to automatically trigger every 5 s, and the thermal camera was configured to capture frames every 2 s. The ground sample distance (GSD) was about 3.9 cm and 12.2 cm for multispectral and thermal sensors, respectively. Multispectral images are single frame, while for thermal data collection the area of study was captured in sets of two or more images, due to limited field of view of the FLIR Tau 2 camera. In 2015, the genotypes were planted on 20 May; while the genotypes were planted on 8 June in 2016. In 2015, the data was collected at about 50, 60, and 75 days after planting (DAP), corresponding to the dates 8 July (49 DAP), 20 July (61 DAP), and 31 July (72 DAP). In 2016, data was collected at around 60 and 75 DAP on 9 (62 DAP) and 26 August (79 DAP). In 2015, the growth stages during data collection were at R1 (bloom beginning), R3 (50% bloom), and R5 (beginning of seed development); while in 2016, the growth stages were at R5 and R8 (beginning of maturity). The growth stages were defined based on dry bean growth staging guide provided by Manitoba Pulse and Soybean Growers (2019). For simplicity, the data collection dates are referred as 50, 60, and 75 DAP. Thermal data was collected only at about 60 and 75 DAP in both years. In addition, from the original features extracted with UAS multispectral images (3.9 cm), lower resolution images (GSD = 0.05, 0.1, 0.2, 0.5, 1.0, 2.0, 3.0 and 5.0 m) were generated to simulate satellite imagery and evaluate their potential in crop performance assessing for breeding programs.

2.3. Satellite data acquisition

Four high spatial resolution satellite images were used from different sources (resolution in parenthesis): Pleiades-1A (0.5 m), SPOT 6 (1.5 m), Planet Scope (3.0 m), and Rapid Eye (level 3A, 5.0 m). Except Planet Scope data, images from the other sources have four bands in common: R, G, blue (B), and NIR. Additionally, Rapid Eye images have a red edge band, while Pleiades-1A and SPOT 6 contain a high spatial resolution panchromatic band. Although the Planet Scope images generally contains NIR information, the scene used in this research

contain only blue, green and red bands (Supplementary Materials, Table S3).

The panchromatic image is a single band raster file with a wide width band of approximately 350 nm. For Pleiades-1A and SPOT 6 data, the panchromatic band is used to increase the spatial resolution of multispectral data through a process known as panchromatic sharpening, or pan-sharpening. The R, G, B and NIR channels of Pleiades-1A have an original resolution of 2.0 m, which after pan-sharpening increases up to the panchromatic band spatial resolution of 0.5 m. Employing this process to SPOT 6 imagery, the original data resolution increased from 6.0 m up to 1.5 m. Pan-sharpening was not required for Planet Scope and Rapid Eye imagery.

The selection of the satellite images used for evaluation and validation was based on availability and temporal proximity to UAS data collection dates. Such data was only available for year 2016. Pleiades-1A and SPOT 6 images were at 22 and 13 days before UAS data collection at about 60 DAP, respectively; whereas, the Planet Scope and Rapid Eye images were 5 and 9 days before UAS data collection at about 75 DAP, respectively (Supplementary Materials, Fig. S2).

2.4. Image processing and analysis

2.4.1. UAS-based multispectral image analysis

The multispectral images were radiometrically corrected, and then georeferenced. For radiometric correction of multispectral data, the images were normalized by setting the reference panel image pixels to the maximum gray level of 255 (individual bands), as it reflects 99% of the visible (R-G-B) and NIR radiation. The georeferencing was done in QGIS (QGIS Development Team, 2018) with the "Georeferencer" tool. Using this tool, the original image was placed on its correct geographical location based on coordinate identification of common objects (corners of the study area) between the UAS image and a reference map (Google Hybrid map). No stitching process was required as the images captured all the plots in the field. From the pre-processed multispectral images, three vegetation index (VI) images were generated; namely, Normalized Difference Vegetation Index (NDVI, Eq. (1)), Green Normalized Difference Vegetation Index (GNDVI, Eq. (2)), and Soil Adjusted Vegetation Index (SAVI, Eq. (3)). In addition, an image was generated by thresholding the SAVI map to estimate Canopy Cover. The canopy cover for individual plots was estimated using Eq. (4), by computing the total number of pixels above the set threshold.

$$NDVI = \frac{NIR - R}{NIR + R} \tag{1}$$

$$GNDVI = \frac{NIR - G}{NIR + G} \tag{2}$$

$$SAVI = \frac{NIR - R}{(NIR + R + L)} * (1 + L) \tag{3}$$

$$Canopy\ cover = \sum_{i=1}^{n} DNcov_i, If = \begin{cases} NDVI < threshold \Rightarrow DN_{Cov} = 0 \\ NDVI \geq threshold \Rightarrow DN_{Cov} = 1 \end{cases} \tag{4}$$

where R, G and NIR indicate the reflectance (pixel value or digital number/DN) of the red, green and infrared bands. SAVI was calculated to minimize the influence of soil brightness (Huete, 1988) for comparison with NDVI and GNDVI. For 2015 at about 50 DAP and 60 DAP, and 2016 at about 75 DAP, the threshold (L) was set as 0; while, at about 75 DAP in 2015 and 60 DAP in 2016, L was set as 0.1. DN data with equal or higher values than the thresholds were considered as vegetation cover ($DN_{cov} = 1$), and pixels below that level were identified as non-vegetation cover ($DN_{cov} = 0$). The canopy cover was estimated as the sum (SUM) of all the pixels considered as vegetation cover inside one plot. To avoid interferences from soil pixels, the NDVI, GNDVI and SAVI features were extracted inside the vegetation canopy cover areas.

In a GIS environment, the boundary of all plots was digitalized in a polygon layer. To avoid border effects, the polygon surrounds each plot at 30 cm inwards from the boundary. Utilizing the "Zonal Statistic" tool of QGIS, the average (MEAN) values of the image features were recorded as an attribute in the polygon layer. This attribute table was exported in a text (*.txt) file, where it was linked with the ground truth of each polygon through a specific plot ID. This ID coded for year, DAP, experiment and plot number, and facilitated subsequent statistical analyses.

2.4.2. UAS-based thermal image analysis

The MEAN canopy temperature was extracted from images in two ways: (a) with raw data (non-normalized), and (b) through normalization. During normalization, the thermal image pixel data (temperature) were adjusted based on five common plots captured in all the images within a data collection period. One image was set as reference, to extract the average temperature of these plots. The data was also extracted from other images (that need to be corrected) and a correction factor was computed based on the average differences between MEAN temperature with respect to the reference. Finally, the MEAN temperature from both normalized and non-normalized images was extracted per plot to the polygon layer. The MEAN temperature values were associated to each plot based on the specific ID described above. Finally, the MEAN temperature data was estimated using thermal images (non-normalized/normalized) were correlated with seed yield and biomass.

2.4.3. Satellite imagery analysis

Satellite images must be first corrected to attenuate the atmospheric distortion due to the presence of particles like aerosols, gases, and moisture (Jensen, 2005; Rotta et al., 2016). Rapid Eye, SPOT 6, and Pleiades-1A images were provided by the supplier with the atmospheric correction. To perform the atmospheric correction (at the top of the atmosphere) of Planet Scope images, each band is multiplied by a specific factor of correction that is recorded in a metadata (*.xml) file. As this information was not present in the metadata file of the image used in this study, the raw image data was used. The pan-sharpening is a resolution merging method in image processing. In this technique, a high resolution panchromatic (single band) image is merged with a lower resolution multispectral (multi-band) dataset. The result is a multispectral image conserving its spectral information, but with the high spatial resolution of the panchromatic band (Grochala and Kedzierski., 2017). This processing was done with Pleiades-1A and SPOT 6 images, increasing the original spatial resolution of the multispectral images from 2.0 m and 6.0 m up to 0.5 and 1.5 m, respectively. Although the satellite images are orthorectified and georeferenced, they have position errors in the order of several meters (Cuartero et al., 2014). In the present study, the geo-location was corrected to avoid position errors in plots from the satellite images. This correction was performed in the QGIS with the "Georeferencer" tool. Finally, the mean NDVI values of Pleiades-1A, SPOT 6 and Rapid Eye were recorded in the polygon layer (previously created) and linked with the respective ground truth data based on the same specific ID. Since the Planet Scope image did not have the NIR band, the feature extracted was the Green Red Vegetation Index (GRVI, Bendig et al., 2015) (Eq. (5)).

$$GRVI = \frac{Green - Red}{Green + Red} \tag{5}$$

2.5. Statistical analysis

For Pearson's correlations analysis, R Studio (version 3.6.0, R Studio Inc., Boston, MA, USA) was used. Multispectral image features were correlated with emergence, biomass, CH, DHM, DF and seed yield on an individual plot basis. Thermal and satellite image-based features were correlated with biomass and seed yield on an individual plot basis.

3. Results

3.1. Relationship between UAS-based multispectral image features with performance and phenological traits

Table 2 summarizes the correlations between the performance traits (emergence, biomass, seed yield) and the image features (NDVI, GNDVI, SAVI and canopy cover). As a group, the ADP is inherently more sensitive to stress than the DDP; therefore, exhibits wider variation in performance traits. This likely contributed to the stronger correlations observed for performance traits with image features in ADP. The increased variation in the ADP results in part from an even mix of different growth habits, as determinate bush and indeterminate vine types were included among the genotypes in the panel. Conversely, the DDP is comprised of genotypes with predominately indeterminate vine types that vary from prostrate, semi-upright, to upright growth habits.

For 50 DAP, the correlations between image features and the three performance traits (emergence, biomass, seed yield) were low ($r = |0.18|$ to $|0.50|$) or non-significant (e.g. seed yield with GNDVI and canopy cover in DDP, 2015). With few exceptions, negative correlations were observed for emergence and biomass with image features because the ratings are inversed such that as emergence and biomass increased, the rating scores decreased, and the image feature values (VIs and canopy cover) increased. For emergence (stand establishment), overall stronger correlations with image features (NDVI, GNDVI) were observed for the ADP than the DDP. The highest correlations among traits were observed for biomass with image features, and similarly slightly

Table 2
Correlation coefficients (r) by experiment between performance traits (emergence, biomass, seed yield) and multispectral image features (NDVI, GNDVI, SAVI, canopy cover) at about 50, 60 and 75 DAP in 2015, and about 60 and 75 DAP in 2016. * represents p < 0.05, ** represents p < 0.01, and *** represents p < 0.001.

DAP	Panel	Emergence				Biomass				Seed yield			
		NDVI	GNDVI	SAVI	Canopy cover	NDVI	GNDVI	SAVI	Canopy cover	NDVI	GNDVI	SAVI	Canopy cover
2015													
50	DDP	− 0.27***	− 0.23***	− 0.27***	− 0.18***	− 0.28***	− 0.19***	− 0.28***	− 0.19***	0.19***	0.07	0.19***	0.07
	ADP	− 0.47***	− 0.45***	− 0.47***	− 0.43***	− 0.49***	− 0.48***	− 0.49***	− 0.50***	0.38***	0.44***	0.38***	0.43***
60	DDP	− 0.18***	− 0.19***	− 0.18***	− 0.25***	− 0.55***	− 0.42***	− 0.55***	− 0.25***	0.48***	0.33***	0.48***	0.18***
	ADP	− 0.40***	− 0.43***	− 0.40***	− 0.41***	− 0.67***	− 0.57***	− 0.67***	− 0.51***	0.53***	0.54***	0.53***	0.44***
75	DDP	− 0.10	− 0.10*	− 0.10	− 0.10*	− 0.66***	− 0.61***	− 0.66***	− 0.56***	0.58***	0.52***	0.58***	0.49***
	ADP	− 0.25***	− 0.26***	− 0.25***	− 0.25***	− 0.78***	− 0.71***	− 0.78***	− 0.67***	0.51***	0.52***	0.51***	0.47***
2016													
60	DDP	− 0.11	− 0.06	− 0.11	< 0.01	− 0.72***	− 0.36***	− 0.73***	< 0.01	0.42***	− 0.10	0.42***	< 0.01
	ADP	− 0.50***	− 0.51***	− 0.50***	− 0.40***	− 0.91***	− 0.83***	− 0.91***	− 0.27**	0.73***	0.63***	0.73***	0.30**
75	DDP	0.27***	0.23**	0.27***	0.27***	− 0.58***	− 0.57***	− 0.58***	− 0.64***	− 0.03	− 0.01	− 0.03	0.01
	ADP	− 0.23*	− 0.24*	− 0.23*	− 0.28**	− 0.69***	− 0.69***	− 0.69***	− 0.70***	0.64***	0.64***	0.64***	0.55***
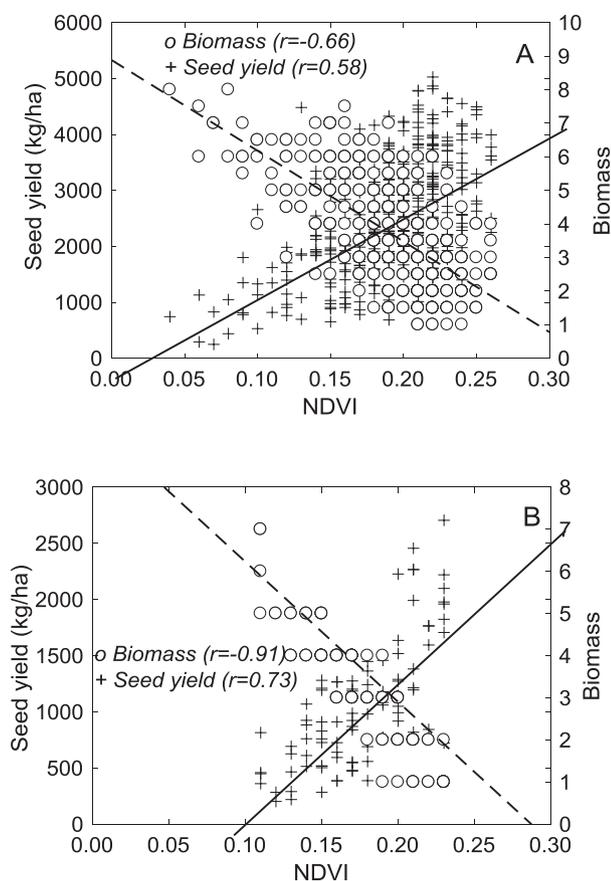
Fig. 1. Correlation of NDVI with biomass and seed yield at (A) 75 DAP with DDP genotypes in 2015, and (B) 60 DAP with ADP genotypes in 2016.

weaker correlations were observed in the DDP compared to ADP (Fig. 1). Interestingly the correlation of biomass and seed yield was similar between NDVI and SAVI, given that SAVI is a variant of NDVI, this could be expected. GNDVI correlations with biomass and seed yield were marginally lower than NDVI and SAVI. In general, the correlation between biomass and canopy coverage was highest at 75 DAP, in both panels and in both years. Emergence and biomass scores were less variable in DDP than ADP which likely contributed, in part, to the slightly weaker correlations with VIs in the DDP versus the ADP.

The correlations of increasing seed yield with higher image data values were significant in most cases, slightly stronger in the ADP than

DDP, more consistent across panels in 2015 than 2016 (which experienced greater stress than 2015), and weaker at 50 DAP in comparison to 60 DAP or 75 DAP (Fig. 1). Given the sensitivity of ADP genotypes to stress, the correlations with seed yield were higher in 2016 than 2015. Non-significant correlations occurred between seed yield and VIs (excluding NDVI and SAVI at 60 DAP) in DDP at 60 and 75 DAP in 2016, while the reverse was observed for the ADP (significant correlations between seed yield and VIs).

Phenology traits (DF, DHM and CH) correlations with image data were much lower or non-significant in 2015 than in 2016 (Table 3). Most of these correlations were in the positive direction except for DDP in 2015. In both panels, correlations between image features with phenological traits (DF, DHM, CH) were stronger in 2016, especially at 75 DAP (e.g. Fig. 2). This may have been influenced by earlier flowering and maturing genotypes, whereas later flowering and maturing and taller genotypes generated more biomass as supported by the positive correlation with image features. Compared to 2015, plant growth cycle was also compressed in 2016, due to the later planting date. With the expanded growth cycle in 2015, later flowering and maturing genotypes took longer to generate canopy coverage/biomass.

3.2. Relationship between UAS-based thermal data with performance traits

The relationship between UAS-based thermal data with biomass and seed yield was examined. In general, the correlations between MEAN temperatures extracted using two different methods (with and without normalization) and biomass were stronger than those obtained with seed yield (Table 4). Increasing biomass (lower scores) was correlated ($r = 0.20$–0.88) with lower MEAN thermal temperatures, using thermal data extracted from images without normalization. Lower seed yield was consistently correlated with higher temperatures. These correlation coefficients between the seed yield and biomass with MEAN temperature under multiple stress were comparable or higher than those found in terminal drought stress dry bean experiments ($r = 0.33$ with biomass and -0.34 with seed yield under stressed conditions) as reported in Sankaran et al. (2018).

One of the major purposes for thermal data analysis was to develop a reliable method to extract temperature data associated with canopy performance. The correlation coefficients between biomass or seed yield with MEAN temperature extracted from non-normalized and normalized images did not differ except 75 DAP in DDP panel in 2015. This change may have resulted from variability in the temperature (weather) occurring on the day of data collection, as this effect was only found in DDP at 75 DAP in 2015. The ADP was not affected as the genotypic data were acquired from a single image. This indicates that such normalization of thermal data using a reference thermal image

Table 3

Correlation coefficients (r) by experiment between phenological traits (days to 50% flowering-DF, days to harvest maturity-DHM, and canopy height –CH) and multispectral image features (NDVI, GNDVI, SAVI, canopy cover) at about 50, 60 and 75 DAP in 2015, and about 60 and 75 DAP in 2016. * represents $p < 0.05$, ** represents $p < 0.01$, and *** represents $p < 0.001$.

DAP	Panel	DF				DHM				CH			
		NDVI	GNDVI	SAVI	Canopy cover	NDVI	GNDVI	SAVI	Canopy cover	NDVI	GNDVI	SAVI	Canopy cover
2015													
50	DDP	−0.01	−0.09	−0.01	−0.13**	−0.02	−0.02	−0.02	−0.05	−0.16**	−0.06	−0.16**	−0.04
	ADP	0.04	−0.01	0.04	−0.01	−0.17*	−0.20**	−0.17*	−0.19**	0.15*	0.12	0.15*	0.12
60	DDP	0.15**	0.14**	0.15**	0.01	0.05	0.09	0.05	0.04	−0.14**	−0.02	−0.14**	−0.06
	ADP	0.11	0.03	0.11	−0.04	−0.06	−0.14	−0.06	−0.16*	0.25***	0.20**	0.25***	0.17*
75	DDP	0.16**	0.15**	0.16**	0.08	0.20***	0.22***	0.20***	0.15**	−0.26***	−0.19***	−0.26***	−0.21***
	ADP	0.20**	0.14*	0.20**	0.11	0.14*	0.08	0.14*	0.04	0.40***	0.36***	0.40***	0.31***
2016													
60	DDP	0.33***	0.32***	0.33***	< 0.01	0.28***	0.22**	0.28***		0.26**	0.39***	0.26**	< 0.01
	ADP	0.36***	0.26*	0.36***	−0.04	0.54***	0.45***	0.54***	0.08	0.60***	0.54***	0.60***	0.09
75	DDP	0.65***	0.62***	0.65***	0.62***	0.88***	0.84***	0.88***	0.80***	0.35***	0.32***	0.35***	0.32***
	ADP	0.41***	0.39***	0.41***	0.43***	0.72***	0.68***	0.72***	0.71***	0.47***	0.46***	0.47***	0.49***
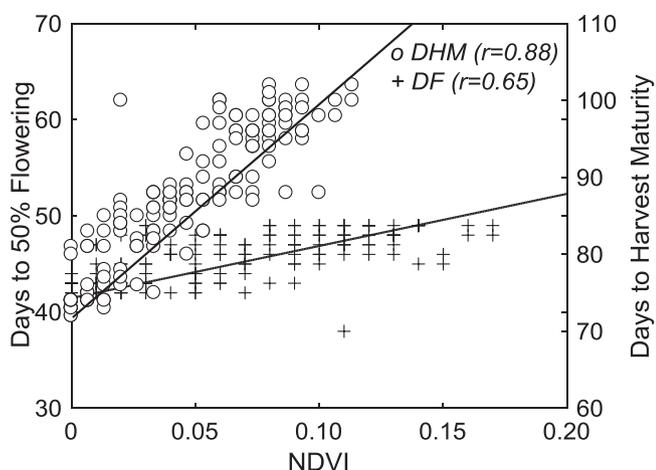
Fig. 2. Correlations of NDVI with days to 50% flowering (DF) and days to harvest maturity (DHM) in DDP at 75 DAP in 2016.

Table 4
Correlations between yield and seed biomass with MEAN temperature extracted from normalized and non-normalized thermal images at 60 and 75 DAP. * represents $p < 0.05$, ** represents $p < 0.01$, and *** represents $p < 0.001$.

Year	DAP	Exp.	Biomass	Seed yield	Biomass	Seed yield
Raw image data			Non-normalized		Normalized	
2015	60	DDP	0.54***	−0.59***	0.52***	−0.57***
		ADP	0.66***	−0.31**	0.66***	−0.31**
	75	DDP	0.20***	−0.23***	0.43***	−0.42***
		ADP	0.62***	−0.56***	0.62***	−0.56***
2016	60	DDP	0.27*	−0.27*	0.28*	−0.29*
		ADP	0.88***	−0.79***	0.88***	−0.79***
	75	DDP	0.71***	−0.28***	0.76***	−0.33***
		ADP	0.77***	−0.69***	0.77***	−0.69***

could be effective in eliminating the environmental effects on temperature measurements. Further studies are needed to validate this method alongside microclimate data. In general, higher correlations between MEAN temperature with biomass and seed yield were found with ADP at both dates, especially in 2016 (Fig. 3).

3.3. Relationship between UAS-based simulated and original satellite images with performance traits

Satellite imagery has been widely used for agriculture applications all around the world; nevertheless, the applicability of this technology for plant phenotyping has not been explored. In recent years, new satellite data from multiple sources with high resolution imagery between 0.4 m and 3.0 m are available. The higher resolution data offers the exploration of satellite imagery in plant phenotyping applications. In this study, we performed a test evaluation of applicability of satellite imaging for plant phenotyping applications by reducing the UAS data image resolution to simulate satellite images, and then validated our findings with actual satellite images. As a first step, the UAS image resolution was reduced up to 5.0 m (60 DAP, 2016) and the correlations between average NDVI with seed yield and biomass were computed (Fig. 4).

The results showed that the correlation between seed yield and biomass with NDVI begin to decrease at 1.0 m image resolution (although significant). The correlation coefficients reduced from 0.66 to 0.38 with seed yield, and from −0.82 to −0.54 with biomass, with a decrease from 0.5 m/pixel to 1/pixel resolution in ADP. At 2.0 m, similar correlation coefficients were acquired, that remained significant with biomass and seed yield in ADP. These results suggest that images with a pixel resolution up to 1.0 m can sustain the relationship between
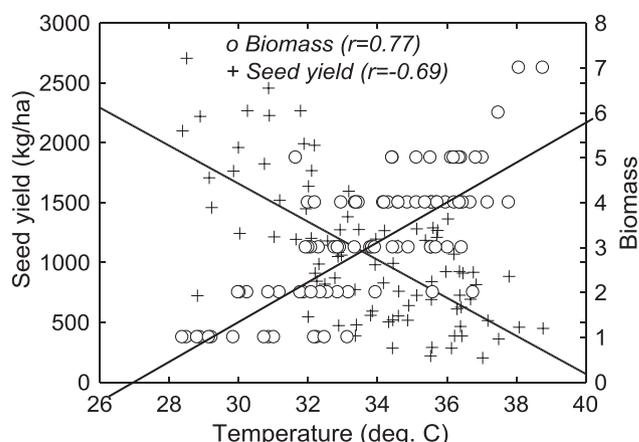
Fig. 3. Correlation of MEAN temperature from normalized images with seed yield and biomass (ADP genotypes) at 75 DAP in 2016.

remote sensing data features such as NDVI and ground reference data (biomass, seed yield). This is especially true for phenotyping applications in breeding programs, where research plots are smaller. Depending on crop and size of plots, the findings can vary. At 3.5 m and 5.0 m image resolution, the correlation between NDVI with seed yield and biomass was considerably reduced and non-significant. Similar to high-resolution UAS data, the correlation between NDVI and biomass were stronger than with seed yield.

For the satellite data, four images were acquired with resolutions of 0.5 m (Pleiades-1A), 1.5 m (Spot 6), 3.0 m (Planet), and 5.0 m (Rapid Eye) at DAP close to UAS data collection in 2016 (Supplementary Materials, Fig. S3). The average NDVI was extracted from each satellite image and the data were correlated with seed yield and biomass (Table 5). In general, for the ADP, higher correlations were obtained with the Pleiades-1A image for both biomass ($r = -0.55$) and seed yield ($r = 0.52$) traits, and comparable r values were observed with SPOT 6 image. Conversely, for DDP, the highest correlations with biomass ($r = -0.31$) and seed yield ($r = 0.34$) were solely obtained with SPOT 6 image data. The effect of reducing resolution in ADP was found to be lower, likely because the higher variability among genotypes retained performance differences at different growth stages. The lower correlations with satellite images than predicted with simulated satellite images may be due to the time gap between satellite and UAS data capture. The images with higher resolution, i.e. Pleiades-1A and SPOT 6, were available at 23 and 14 days (respectively) before the UAS data collection at 62 DAP in 2016. The image from Rapid Eye was captured closer to that time point, only 8 days after. The Planet Scope data was from 5 days before the UAS data collection at 79 DAP.

The lower correlations between image features extracted from Planet Scope image (3.0 m) and performance traits may result from using a different image feature (GRVI) necessitated by absence of the NIR band in the unique image available during the time when this research was performed. The wider time gap between the date of acquisition of Pleiades-1A and the UAS would expect to result in lower r values obtained with the satellite image than predicted UAS image. Overall, these findings support the use of high resolution satellite imagery for phenotyping application.

4. Discussion and summary

The response of bean plants to drought conditions is complex involving several physiological mechanisms related to energy metabolism, photosynthesis, energy conversion, protein synthesis and proteolysis (Zadražnika et al., 2013, 2017). Drought can negatively affect the dry matter production, number of pods per plant, number of seeds, hundred seed weight and grain yield (Mathobo et al., 2017). Drought
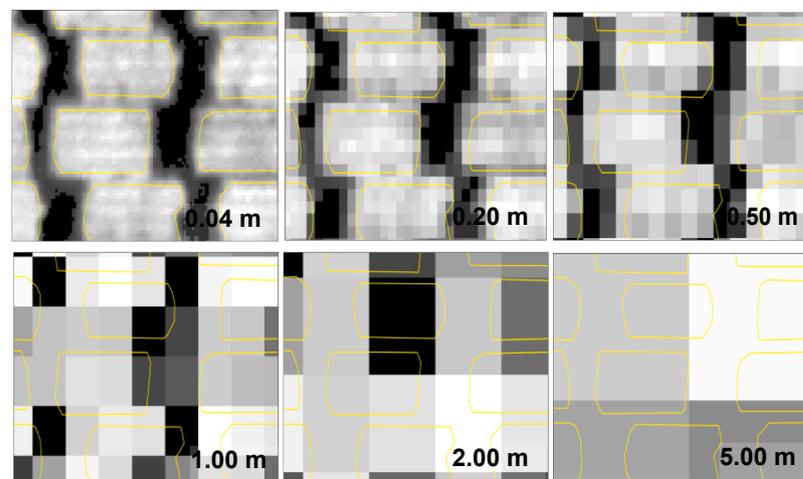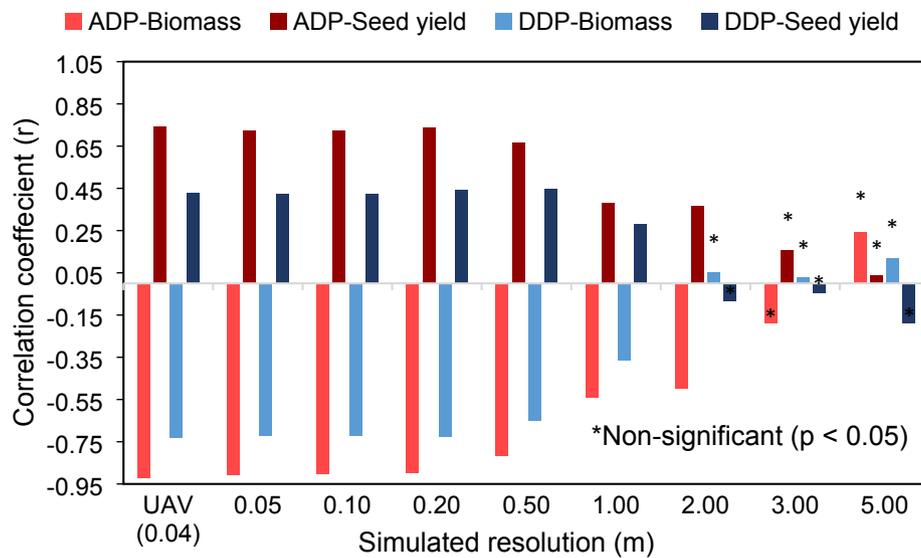
Fig. 4. Correlation between biomass and seed yield with NDVI in ADP and DDP at 60 DAP, for simulated decreasing resolutions of the original UAS image.

Table 5
Correlations between seed yield and biomass with NDVI from Pleiades-1A, Spot 6, and Rapid Eye images, and with SR from Planet image. * represents $p < 0.05$, ** represents $p < 0.01$, and *** represents $p < 0.001$.

Trait	Panel	UAS (3.9 cm) 60 DAP	Pleiades-1A (0.5 m) 38 DAP	SPOT 6 (1.5 m) 47 DAP	Rapid Eye (5.0 m) 66 DAP	UAS (3.9 cm) 75 DAP	Planet (3.0 m) 70 DAP
Biomass	DDP	−0.72***	−0.11	−0.32***	−0.12	−0.58***	< 0.01
	ADP	−0.91***	−0.55***	−0.50***	−0.48***	−0.69***	−0.36***
Seed yield	DDP	0.42***	0.17*	0.35***	0.19*	−0.03	−0.09
	ADP	0.73***	0.52***	0.45***	0.48***	0.64***	0.33**

tolerant cultivars more effectively partition carbohydrates toward seed filling under stress conditions, prioritizing seed production over leaf development (Rosales et al., 2012). But biomass is necessary to realize yield; thus, genotypes that generate more biomass can be more drought tolerant. The remote sensing data indicated that the DDP accumulated more biomass compared with ADP, leading to higher yields under stress.

The beans of Race Durango origin have been identified as an important genetic source of drought tolerance. Rosales et al. (2012) observed that Pinto Saltillo (Durango cultivar) maintained productivity under terminal drought conditions. Compared with Durango race, Andean beans are more sensitive to drought stress. Herein, for the ADP, where lower vigor plots prevailed, higher correlations between biomass

and seed yield with image features were found, as similarly observed by Sankaran et al. (2018). Differences in vegetation index values are enhanced under low vigor conditions, which likely contributed to the stronger correlations observed for the ADP. The results from this study and those of Sankaran et al. (2018) support multispectral imaging at 60–75 DAP to capture differences in performance traits such as biomass and seed yield.

Modified RGB cameras are low-cost multispectral cameras that enable capture of NIR spectral reflectance (in addition to a couple visible bands). These sensors are used in agricultural research (Quiros et al., 2019; Putra and Soni, 2017; Zhang et al., 2017; Sankaran et al., 2015 a, b; Hunt et al., 2011) with promising results. Although limited by spectral resolution, these sensors provide high spatial resolution data

similar to the original RGB sensors (Elarab et al., 2015). However, these broad spectral resolution sensors may have large variability in spectral response; thus, vegetation indices derived from them need to be carefully analyzed, in comparison to 'true' multispectral data. The sensitivity of sensor-based evaluation may be enhanced using narrow-band multispectral cameras, but this needs to be further assessed. The narrow-band multispectral camera (with 5–12 bands) also offers extraction of several vegetation indices that may enhance the phenotyping potential.

In agriculture, thermal data have been used for drought stress monitoring (Gerhards et al., 2016; García-Tejero et al., 2016, 2018; Biju et al., 2018) and disease detection (Baranowski et al., 2015). Tu and Tan (1985) studied the leaf temperature in diseased bean plants with and without drought conditions, and found that changes in temperature were more prevalent under drought. The correlations obtained herein between remote sensed average canopy temperature (60–75 DAP) and seed yield were comparable or higher than those observed by Sankaran et al. (2018). Furthermore, similar to multispectral image features, the correlations of temperature data from thermal images with performance traits in ADP were stronger, which may result in part from its greater sensitivity to drought conditions as described above. Given the dynamic nature of canopy temperature measurement, which is affected by environment (soil exposure, wind, cloud cover, etc.), the application of field sensing can be challenging. A common normalization method is to convert thermal data into crop water stress index/CWSI (García-Tejero et al., 2016; Bai et al., 2017). Many researchers have proposed multiple ways of computing CWSI. Gomez-Candón et al. (2016) tested a radiometric calibration method, for multi-temporal data comparisons, based on the temperature of ground reference objects measured with thermo-radiometers. However, such approaches under field conditions are time-consuming. Therefore, we developed a new normalization method that utilizes common plots between two images. Although the actual canopy measure is hard to predict, the method showed potential to delineate performance differences between genotypes. This normalization method was better associated with performance traits than CWSI-based normalization. Further validation with microclimate data is needed to implement this method in field phenotyping.

UAS-based remote sensing for high-throughput phenotyping in the field is becoming more plausible, and provides numerous advantages related to high spatial and temporal resolutions. Nevertheless, the use of UAS poses challenges such as the need for and timing of several field visits, training to operate and acquire reliable data, etc. Our examination of simulated satellite images derived from UAS, found that image resolutions up to 1 m per pixel may be useful in providing quality data for reliable biomass and seed yield performance evaluation. Perhaps a lower resolution image may be applicable in different crops with larger plot sizes.

NDVI from Pleiades-1A (0.5 m) and SPOT 6 (1.5 m) satellite images were associated with performance in the ADP. NDVI from Planet Scope (3.0 m) and Rapid Eye (5.0 m) images were less related to biomass and seed yield, and likely will require higher resolution for reliable prediction of crop performance. The usefulness of sub-meter satellite imagery relies on the size of the study objects (monitoring the variability of crop biophysical traits at parcel level as in Liu et al., 2018). Schut et al. (2018), using the same source of satellite imagery, compared the satellite VI data with the UAS data in 15 m × 15 m plots (more than 40 times the size of the breeding plots analyzed in the present study) and reported that the satellite image was able to capture the intra-plot variability at the accuracy level of UAS. Our work shows that higher resolution low-orbiting satellite images are promising for high-throughput field phenotyping, and offer a reliable and practical solution to acquire multispectral phenotypic data from breeding trials at a desired temporal resolution.

In regard to the multiple sensor data utilized in this study (UAS-based multispectral and thermal, LOS-based multispectral imaging data), each data type was analyzed independently to assess potential for

capturing the phenotypic differences based on crop responses. Among the different traits, the differences in biomass and seed yield potential were captured most effectively using the remote sensing data. Similarly, remote sensing data were able to capture the differences in phenotypic responses, especially in ADP panel, where the genotypes were more sensitive to crop stress. Thus, remote sensing techniques may be more applicable at early stages of breeding cycles, when there are more genotypes sensitive to stress. Both UAS-multispectral (e.g. NDVI, SAVI) and thermal data were able to capture the differences in phenotypic responses, as indicated by the strong correlations between this data and phenotypic traits such as biomass and seed yield. In general, multispectral features show strong relationships with agronomic traits (e.g. Quiros et al., 2019). However, differences in architectural status (leaf type, canopy type) may influence the multispectral data and can mask the differences in agronomic performance in crops, especially if the performance (seed yield, biomass) is not associated with architectural status. In such cases, thermal data offers robust capture of performance traits. Breeders are interested in thermal data, based on its strong association with physiological traits such as stomatal conductance and transpiration rate. The higher resolution LOS multispectral data (0.5–1.0 m/pixel) showed potential for capturing phenotypic differences, and coordinated timing of data acquisition at key phenological stages of crop growth will likely enhance its applications. Towards the future, data fusion from multiple sources (UAS-based multispectral and thermal, LOS-based multispectral imaging data), although unexplored in this study, will be integrated with machine learning tools for selection of breeding lines.

Appendix A. Supplementary material

Supplementary data to this article can be found online at https://doi.org/10.1016/j.compag.2019.104965.

References

Abrahão, S., de Carvalho, F., de Queiroz, D., Terra, N., Souza, J., 2013. Determination of nitrogen and chlorophyll levels in bean-plant leaves by using spectral vegetation bands and indices. Centro de Ciências Agrárias, Universidade Federal do Ceará. 44 (3), 464–473. https://doi.org/10.1590/S1806-66902013000300007.

Andrade-Sanchez, P., Gore, M.A., Heun, J.T., Thorp, K.R., Carmo-Silva, A.E., French, A.N., White, J.W., 2014. Development and evaluation of a field-based high-throughput phenotyping platform. Funct. Plant Biol. 41 (1), 68–79. https://doi.org/10.1071/FP13126.

Bai, J.J., Yu, Y., Di, L., 2017. Comparison between TVDI and CWSI for drought monitoring in the Guanzhong Plain, China. J. Integrative Agric. 16 (2), 389–397. https://doi.org/10.1016/S2095-3119(15)61302-8.

Baranowski, P., Jedryczka, M., Mazurek, W., Babula-Skowronska, D., Siedliska, A., Kaczmarek, J., 2015. Hyperspectral and thermal imaging of oilseed rape (*brassica Brassica napus*) response to fungal species of the genus alternaria. Biosyst. Eng. 10, 1–19. https://doi.org/10.1371/journal.pone.0122913.

Beebe, S.E., Rao, I.M., Blair, M.W., Acosta-Gallegos, J.A., 2013. Phenotyping common beans for adaptation to drought. Front. Physiol. 4. https://doi.org/10.3389/fphys.2013.00035.

Bendig, J., Kang, Y., Aesen, H., et al., 2015. Combining UAV-based plant height from crop surface models, visible, and near infrared vegetation indices for biomass monitoring in barley. Int. J. Appl. Earth Obs. Geoinf. 39, 79–87. https://doi.org/10.1016/j.jag.2015.02.012.

Biju, S., Fuentes, F., Gupta, D., 2018. The use of infrared thermal imaging as a non-destructive screening tool for identifying drought-tolerant lentil genotypes. Plant Physiol. Biochem. 127, 11–24. https://doi.org/10.1016/j.plaphy.2018.03.005.

Boechat, L.T., Pinto, F.D.A.D.C., Júnior, P., Queiroz, D.M., Teixeira, H., 2014. Detection of white mold on dry beans using spectral characteristics. Revista Ceres. 61 (6), 907–915. https://doi.org/10.1590/0034-737X201461060004.

Cichy, K., Porch, T., Beaver, J.S., Cregan, P., Fourie, D., Glahn, R., Grusak, M., Kamfwa, K., Katuuramu, D., McClean, P., Mndolwa, E., Nchimbi-Msolla, S., Pastor-Corrales, M., Miklas, P.N., 2015. A *Phaseolus vulgaris* diversity panel for Andean bean improvement. Crop Sci. 55, 1–12. https://doi.org/10.2135/cropsci2014.09.0653.

Cuartero, A., Felicísimo, A.M., Polo, M.E., Caro, A., Rodríguez, P.G., 2014. Positional accuracy analysis of satellite imagery by circular statistics. Photogramm. Eng. Remote Sens. 11, 1275–1286. https://doi.org/10.14358/PERS.76.11.1275.

Elarab, M., Tlicavilca, A.M., Torres-Rua, A.F., Maslova, I., McKee, M., 2015. Estimating chlorophyll with thermal and broadband multispectral high resolution imagery from an unmanned aerial system using relevance vector machines for precision agriculture. Int. J. Appl. Earth Observ. Geoinf. 43, 32–42. https://doi.org/10.1016/j.jag.2015.03.017.

García-Tejero, I.F., Costaac, J.M., Egiptoc, R., Durán-Zuazo, V.H., Lima, R.S.N., Lopes, C.M., Chaves, M.M., 2016. Thermal data to monitor crop-water status in irrigated Mediterranean viticulture. Agric. Water Manag. 176, 80–90. https://doi.org/10.1016/j.agwat.2016.05.008.

García-Tejero, I.F., Gutiérrez-Gordillo, S., Ortega-Arévalo, C., Iglesias-Contreras, M., Moreno, J.M., Souza-Ferreira, L., Durán-Zuazo, V.H., 2018. Thermal imaging to monitor the crop-water status in almonds by using the non-water stress baselines. Sci. Hortic. 238, 91–97. https://doi.org/10.1016/j.scienta.2018.04.045.

Gerhards, M., Rock, G., Schlerf, M., Udelhoven, T., 2016. Water stress detection in potato plants using leaf temperature, emissivity, and reflectance. Int. J. Appl. Earth Obs. Geoinf. 53, 27–39. https://doi.org/10.1016/j.jag.2016.08.004.

Gomez-Candón, D., Virlet, N., Labbé, S., Jolivot, A., Regnard, J.L., 2016. Field phenotyping of water stress at tree scale by UAV-sensed imagery: new insights for thermal acquisition and calibration. Precis. Agric. 17 (6), 786–800. https://doi.org/10.1007/s11119-016-9449-6.

Grochala, A., Kedzierski, M., 2017. A method of panchromatic image modification for satellite imagery data fusion. Remote Sens. 9, 639–660. https://doi.org/10.3390/rs9060639.

Gutierrez, M., Escalante, J., Rodriguez, M., Reynolds, M., 2006. Canopy reflectance indices and its relationships with yield in common bean plants (*Phaseolus vulgaris* L.) with phosphorus supply. Int. J. Agric. Biol. 8 (2), 203–207.

Holman, F.H., Riche, A.B., Michalski, A., Castle, M., Wooster, M.J., Hawkesford, M.J., 2016. High throughput field phenotyping of wheat plant height and growth rate in field plot trials using UAS based remote sensing. Remote Sens. 8 (12), 1031. https://doi.org/10.3390/rs8121031.

Huete, A.R., 1988. A soil-adjusted vegetation index (SAVI). Remote Sens. Environ. 25 (3), 295–309.

Hunt, R.E., Hively, W.D., McCarty, G.W., Daughtry, C., Forrestal, P.J., Kratochvil, R.J., Carr, J.L., Allen, N.F., Fox-Rabinovitz, J.R., Miller, C.D., 2011. NIR-green-blue high-resolution digital images for assessment of winter cover crop biomass. GIScience Remote Sens. 48 (1), 86–98. https://doi.org/10.2747/1548-1603.48.1.86.

Jensen, J.R., 2005. Introductory Digital Image Processing: A Remote Sensing Perspective, third ed. Prentice Hall, Upper Saddle River, NJ.

Jones, H.G., Serraj, R., Loveys, B.R., Xiong, L., Wheaton, A., Price, A.H., 2009. Thermal infrared imaging of crop canopies for the remote diagnosis and quantification of plant responses to water stress in the field. Funct. Plant Biol. 36 (11), 978–989. https://doi.org/10.1071/FP09123.

Liu, W., Huang, J., Chuanwen, W., Xiuzhen, W., Lamin, R.M., Jiahui, H., Dongdong, Z., Yaoliang, C., 2018. Mapping water-logging damage on winter wheat at parcel level using high spatial resolution satellite data. ISPRS J. Photogramm. Remote Sens. 142, 243–256. https://doi.org/10.1016/j.isprsjprs.2018.05.024.

Ludovisi, R., Tauro, F., Salvati, R., Khoury, S., Mugnozza Scarascia, G., Harfouche, A., 2017. UAV-based thermal imaging for high-throughput field phenotyping of black poplar response to drought. Front. Plant Sci. 8, 1681. https://doi.org/10.3389/fpls.2017.01681.

Manitoba Pulse and Soybean Growers, 2019. Available at: https://www.manitobapulse.ca/wp-content/uploads/2017/08/Dry-Bean-Growth-Staging-Guide-_WR.pdf. Accessed on 17 July, 2019.

Mathobo, R., Marais, D., Steyn, J.M., 2017. The effect of drought stress on yield, leaf gaseous exchange and chlorophyll fluorescence of dry beans (Phaseolus vulgaris L.). Agric. Water Manag. 180, 118–125. https://doi.org/10.1016/j.agwat.2016.11.005.

Miklas, P.N., Kelly, J.D., Beebe, S.E., Blair, M.W., 2006. Common bean breeding for resistance against biotic and abiotic stresses: from classical to MAS breeding. Euphytica 147 (1–2), 105–131. https://doi.org/10.1007/s10681-006-4600-5.

Onojeghuo, A.O., Blackburn, G.A., Huang, J., Kindred, D., Huang, W., 2018. Applications of satellite 'hyper-sensing' in Chinese agriculture: challenges and opportunities. Int. J. Appl. Earth Obs. Geoinf. 64, 62–86. https://doi.org/10.1016/j.jag.2017.09.005.

Pengcheng, H.S., Xuemin, W.A., Andries, P., Tao, D., David, J., Yan, G., Bangyou, Z., 2016. Estimation of plant height using a high throughput phenotyping platform based on unmanned aerial vehicle and self-calibration: example for sorghum breeding. Eur. J. Agron. 95, 24–32. https://doi.org/10.1016/j.eja.2018.02.004.

Petry, N., Boy, E., Wirth, J.P., Hurrell, R.F., 2015. The potential of the common bean (*Phaseolus vulgaris*) as a vehicle for iron biofortification. Nutrients 7 (2), 1144–1173. https://doi.org/10.3390/nu7021144.

Polania, J., Rao, I.M., Cajiao, C., Rivera, M., Raatz, B., Beebe, S., 2016. Physiological traits

associated with drought resistance in Andean and Mesoamerican genotypes of common bean (*Phaseolus vulgaris*). Euphytica 210 (1), 17–29. https://doi.org/10.1007/s10681.

Putra, B.T.W., Soni, P., 2017. Evaluating NIR-Red and NIR-Red edge external filters with digital cameras for assessing vegetation indices under different illumination. Infrared Phys. Technol. 81, 148–156. https://doi.org/10.1016/j.infrared.2017.01.007.

QGIS Development Team, 2018. QGIS Geographic Information System. Open Source Geospatial Foundation Project. http://qgis.osgeo.org.

Quiros, J.J., McGee, R.J., Vandemark, G.J., Romanelli, T., Sankaran, S., 2019. Field phenotyping using multispectral imaging in pea (*Pisum sativum* L) and chickpea (*Cicer arietinum* L). Eng. Agric., Environ. Food. https://doi.org/10.1016/j.eaef.2019.06.002. In press.

Rajah, P., Odini, J., Abdel Rahman, E., Mutanga, O., 2017. Determining the optimal phenological stage for predicting common dry bean (*Phaseolus vulgaris*) yield using field spectroscopy. South Africa J. Plant Soil. https://doi.org/10.1080/02571862.2017.1317854.

Rao, I.M., 2014. Advances in improving adaptation of common bean and Brachiaria forage grasses to abiotic stresses in the tropics. In: Handbook of Plant and Crop Physiology. CRC Press, pp. 876–919.

Reza, Md.N., Na, I.N., Baek, S.W., Lee, K.H., 2018. Rice yield estimation based on K-means clustering with graph-cut segmentation using low-altitude UAV images. Biosyst. Eng. https://doi.org/10.1016/j.biosystemseng.2018.09.014.

Rosales, M.A., Ocampo, E., Rodriguez-Valentin, R., Olvera-Carrillo, Y., Acosta-Gallegos, J., Covarrubias, A.A., 2012. Physiological analysis of common bean (*Phaseolus vulgaris* L.) cultivars uncovers characteristics related to terminal drought resistance. Plant Physiol. Biochem. 56, 24–34. https://doi.org/10.1016/j.plaphy.2012.04.007.

Rotta, L., Alcântara, E.H., Watanabe, F., Rodrigues, T., Imai, N., 2016. Atmospheric correction assessment of SPOT-6 image and its influence on models to estimate water column transparency in tropical reservoir. Remote Sens. Appl.: Soc. Environ. 4, 158–166. https://doi.org/10.1016/j.rsase.2016.09.001.

Sankaran, S., Khot, L.R., Carter, A.H., 2015a. Field-based crop phenotyping: multispectral aerial imaging for evaluation of winter wheat emergence and spring stand. Comput. Electron. Agric. 118, 372–379. https://doi.org/10.1016/j.compag.2015.09.001.

Sankaran, S., Khot, L., Zuñiga, C., et al., 2015b. Low-altitude, high-resolution aerial imaging systems for row and field crop phenotyping: a review. Eur. J. Agron. 70, 112–123. https://doi.org/10.1016/j.eja.2015.07.004.

Sankaran, S., Zhou, J., Khot, L.R., Trapp, J.J., Mndolwa, E., Miklas, P.N., 2018. High-throughput field phenotyping in dry bean using small unmanned aerial vehicle based multispectral imagery. Comput. Electron. Agric. 151, 84–92. https://doi.org/10.1016/j.compag.2018.05.034.

Schut, A.G., Traore, P.C.S., Blaes, X., Rolf, A., 2018. Assessing yield and fertilizer response in heterogeneous smallholder fields with UAVs and satellites. Field Crops Res. 221, 98–107. https://doi.org/10.1016/j.fcr.2018.02.018.

Schwalbert, R.A., Amado, T.J., Nieto, L., Varela, S., Corassa, G.M., Horbe, T.A., Rice, C.W., Peralta, N.R., Ciampitti, I.A., 2018. Forecasting maize yield at field scale based on high-resolution satellite imagery. Biosyst. Eng. 171, 179–192. https://doi.org/10.1016/j.biosystemseng.2018.04.020.

Schwartz, H.F. and Langham, M.A.C., 2010. Growth stages of common bean (Phaseolus vulgaris L.). Available in: http://www. ncipmc. org/resources/legume_diagnostic_cards/Legume% 20Diagnostic% 20Cards, 204.

Singh, S., Gepts, P., Debouck, D., 1991. Races of common bean (*Phaseolus vulgaris*, Fabaceae). Econ. Bot. 45, 379–396. https://doi.org/10.1007/BF02887079.

Sugiura, R., Tsuda, S., Tamiya, S., Itoh, A., Nishiwaki, K., Murakami, N., Shibuya, Y., Hirafuji, M., Nuske, S., 2016. Field phenotyping system for the assessment of potato late blight resistance using RGB imagery from an unmanned aerial vehicle. Biosyst. Eng. 148, 1–10. https://doi.org/10.1016/j.biosystemseng.2016.04.010.

Trapp, J., 2015. Genetics of drought tolerance in common bean (Phaseolus vulgaris L.) (Doctoral dissertation). Accessed 5 September 2018.

Trapp, J., Urrea, C.A., Zhou, J., Khot, L.R., Sankaran, S., Miklas, P.N., 2016. Selective phenotyping traits related to multiple stress and drought response in dry bean. Crop Sci. 56, 1460–1472. https://doi.org/10.2135/cropsci2015.05.0281.

Tu, J.C., Tan, C.S., 1985. Infrared thermometry for determination of root rot severity in beans. Centro Internacional de Agricultura Tropical (CIAT). Phytopathology 75 (7), 840–844.

Zadražnika, T., Egge-Jacobsen, W., Meglic, V., Šuštar-Vozlič, J., 2017. Proteomic analysis of common bean stem under drought stress using in-gel stable isotope labeling. J. Plant Physiol. 209, 42–50. https://doi.org/10.1016/j.jplph.2016.10.015.

Zadražnika, T., Hollung, K., Egge-Jacobsen, W., Meglic, V., Šuštar-Vozlič, J., 2013. Differential proteomic analysis of drought stress response in leaves of common bean (*Phaseolus vulgaris* L.). J. Proteomic Anal. 78, 254–272. https://doi.org/10.1016/j.jprot.2012.09.021.

Zaman-Allah, M., Vergara, O., Araus, J.L., Tarekegne, A., Magorokosho, C., Zarco-Tejada, P.J., Olsen, M., 2015. Unmanned aerial platform-based multi-spectral imaging for field phenotyping of maize. Plant Methods 11 (1), 35. https://doi.org/10.1186/s13007-015-0078-2.

Zhang, J., Yang, C., Zhao, B., Song, H., Hoffman, W.C., Shi, Y., Zhang, D., Zhang, G., 2017. Crop classification and LAI estimation using original and resolution-reduced images from two consumer-grade cameras. Remote Sens. 9, 1054. https://doi.org/10.3390/rs9101054.

Zhao, Y., Chen, X., Cui, Z., Lobell, D.B., 2015. Using satellite remote sensing to understand maize yield gaps in the North China Plain. Field Crops Res. 183, 31–42. https://doi.org/10.1016/j.fcr.2015.07.004.